NEW BINARIES IN THE ε CHA ASSOCIATION [*]

César Briceño[1] and Andrei Tokovinin[1]

[1] *Cerro Tololo Inter-American Observatory, Casilla 603, La Serena 1700000, Chile*

ABSTRACT

We present Adaptive Optics-aided speckle observations of 47 young stars in the ε Cha association made at the 4-m Southern Astrophysical Research Telescope in the I band. We resolved 10 new binary pairs, 5 previously known binaries and two triple systems, also previously known. In the separation range between 4 and 300 AU, the 30 association members of spectral types G0 and later host 6 binary companions, leading to the raw companion frequency of 0.010±0.04 per decade of separation, comparable to the main sequence dwarfs in the field. On the other hand, all 5 massive association members of spectral types A and B have companions in this range. We discuss the newly resolved and known binaries in our sample. Observed motions in the triple system ε Cha, composed of three similar B9V stars, can be described by tentative orbits with periods 13 and ∼900 years, and a large mutual inclination.

Keywords: binaries:young

cbriceno@ctio.noao.edu, atokovinin@ctio.noao.edu

Corresponding author: César Briceño

[*] Based on observations obtained at the Southern Astrophysical Research (SOAR) telescope.

1. INTRODUCTION

Multiple star systems are a common product of the process of star formation (Duchêne & Kraus 2013). Characterizing stellar multiplicity in young stellar populations is therefore an important and necessary step toward understanding issues like the fragmentation of primordial cores or massive disks, the early dynamical evolution of stellar systems, the initial mass function of single stars versus multiples, and how stellar multiplicity affects the survival and evolution of circumstellar disks, which bears ultimately on the frequency and properties of planets orbiting binary and multiple star systems (e.g., see review by Reipurth et al. 2014).

Over the past decades we have learned that loose associations like Taurus and Chamaeleon I harbor roughly twice as many low-mass ($M \lesssim 2\,M_\odot$) pre-main sequence binaries than compact clusters of similar age like the Orion Nebula Cluster (ONC), which have multiplicity fractions similar to the field (e.g., Petr et al. 1998; Köhler et al. 2006). These observations can be interpreted with the assumption of an universally high ($\sim 100\%$) primordial multiplicity fraction for all star forming regions, with the subsequent rapid dynamical disruption of binaries in young dense clusters, which significantly lowers the multiplicity fractions (Kroupa 1995; Kroupa et al. 1999; Kroupa & Petr-Gotzens 2011). However, the universality of a high primordial multiplicity fraction, independent of the star forming environment, has lately been questioned and remains debated (King et al. 2012; Marks et al. 2014). Parker & Meyer (2014) find that dynamical processing of populations composed of 100% binaries, even in dense star forming regions, cannot explain the clear differences in the Galactic field binary fraction and mean separation as a function of decreasing primary mass. In summary, there is accumulating evidence that the primordial binary frequency and separation distribution are *not* universal, but may depend on the star forming environment. Therefore it is important to measure multiplicity properties of many young clusters and associations. This work focuses on one such group.

Because of their proximity, the so-called nearby young moving groups (Zuckerman & Song 2004; Torres et al. 2008), like the η Cha cluster (Mamajek et al. 1999) and ϵ Cha association, are excellent laboratories to investigate stellar multiplicity over a wide range of separations. These two stellar aggregates were first proposed by Frink et al. (1998) as a kinematic group of young stars in the general direction of the Chamaeleon dark clouds. Mamajek et al. (2000) discuss ϵ Cha as a sparse association in the context of other nearby stellar systems, and characterize it as a distinct group of 5-15 Myr old stars. Feigelson et al. (2003) derived an age of 3-5 Myr for ϵ Cha. Several recent studies have concentrated on building better membership lists. In their re-examination of the ϵ Cha group membership, Murphy et al. (2013) arrive at a final list of 35-41 members, with a mean distance of 110 ± 7 pc and an age $\sim 3 - 5$ Myr, making it likely the youngest of the nearby moving groups. This is the most complete census of the association available to date; for comparison, Elliott et al. (2015) listed only 24 members of ϵ Cha (17 of them are found in Murphy et al. 2013). Note that attribution of a star to a particular association is complicated because of the partial overlap between young groups; binarity adds yet another complication by distorting photometry and proper motions.

Multiplicity of young stars has been extensively characterized observationally, mostly by high angular resolution imaging (see the review in Duchêne & Kraus 2013). However, ϵ Cha has been largely neglected so far by these studies. The most extensive data are provided by Köhler (2001) who observed X-ray selected young stars in the direction of the dark clouds in Chamaeleon, resolving binaries with separations from $0\rlap{.}''13$ to $6''$. He made no distinction between the more distant Cha I and Cha II groups and the foreground ϵ Cha association; 18 objects of his study overlap with our sample. Köhler found the multiplicity fraction to be comparable to the field. Recently Elliott et al. (2015) probed binarity in ϵ Cha by high-resolution imaging of 10 targets, detecting three binaries. One of those, RXJ1220.4-7407 (KOH 93), was first resolved by Köhler, TYC 9245-535-1 is not featured in our input list, while HD 105923 is independently confirmed by our survey.

Here we present a study of multiplicity of 47 young stars in the direction of the ϵ Cha stellar group; 37 of those are confirmed or candidate members of the association. This is the most extensive search for binaries and multiple systems in ϵ Cha, in the separation range $\sim 0\rlap{.}''04 - 3''$ (equivalent to projected separations $\sim 4 - 300$ AU, assuming a mean distance of 100 pc). In §2 we present the observations, and in §3 our results. Section 4 discusses the multiplicity in ϵ Cha and concludes the paper.

2. OBSERVATIONS

2.1. *Sample Selection*

We used for the target selection the list of proposed members of the ϵ Cha association from the Table 1 of Murphy et al. (2013). Here in Table 1 we provide the characteristics of the 47 observed stars. The members confirmed by Murphy et al. (2013) have their corresponding Cha-NN numbers in column (2); candidate

members are marked as Cha-cand, while the rejected members are labeled as Cha-rej. Columns (2) and (3) contain the star position, columns (5) and (6) the I_c magnitude and Spectral Type respectively, and in columns (7) and (8) we provide distances derived from the *Gaia* DR1 parallaxes (Gaia Collaboration et al. 2016a), and from Murphy et al. (2013). Two candidates, TYC 9414-191-1 and TYC 9420-676-1, can be rejected based on their *Gaia* parallaxes (Lindegren et al. 2016), so their status is set accordingly. On the other hand, HIP 55746 has a *Gaia* parallax of 10.74 mas and is most likely a member of the association; its rejection by Murphy et al. (2013) could have been caused by its close binary companion. For previously known multiples listed in the Washington Double Star Catalog, WDS (Mason et al. 2001), the "discoverer codes" are given in column (2). The separations in column (9) of Table 1 indicate which objects have been resolved; asterisks mark first-time resolutions. Three stars from the original list, 2MJ11334926-7618399, 2MJ11404967-7459394 and 2MJ12014343-7835472, all fainter than $I_c = 14.1$, were not observed and therefore are not included in Table 1.

The final list contains 37 ϵ Cha members/candidates among the 47 entries in Table 1. However, it should be pointed out that the 10 rejected stars are, for the most part, young objects. Their attribution to a particular association or group might be compromised by multiplicity. We believe that their observations are useful regardless of the membership status. Monitoring of known close young binaries will establish their orbits and masses (e.g. EG Cha, Tokovinin 2016).

Table 1. Targets observed in the ϵ Cha stellar group

NAME	Membership	RA(J2000)	DEC(J2000)	I_c	SpT	Distance[a]	Distance[b]	Sep.
	Other ID	(h : m : s)	(° : ′ : ″)	(mag)		(pc)	(pc)	(″)
(1)	(2)	(3)	(4)	(5)	(6)	(7)	(8)	(9)
HD 82879	Cha-rej	09:28:21.1	-78:15:35.0	8.95	F6	111 ± 7	. . .	. . .
CP-68 1388	Cha-22	10:57:49.3	-69:14:00.0	9.28	K1	114 ± 6	112	. . .
VW Cha	Cha-rej; GHE 35	11:08:01.5	-77:42:29.0	11.03	K8	. . .	. . .	0.67
TYC 9414-191-1	Cha-rej	11:16:29.0	-78:25:20.8	9.59	K5	477 ± 157	105	. . .
2MJ11183572-7935548	Cha-13	11:18:35.7	-79:35:54.8	12.22	M4.5	. . .	101	0.92*
RXJ1123.2-7924	Cha-14,rej	11:22:55.6	-79:24:43.8	11.62	M1.5	. . .	. . .	. . .
HIP 55746	Cha-cand	11:25:18.1	-84:57:16.0	7.15	F5	93 ± 6	. . .	0.06*
RXJ1137.4-7648	Cha-rej	11:37:31.3	-76:47:59.0	12.2	M2.2	. . .	. . .	2.89*
TYC 9238-612-1	Cha-rej	11:41:27.7	-73:47:03.0	9.98	G5	158 ± 6	. . .	2.28*
2MJ11432669-7804454	Cha-17	11:43:26.7	-78:04:45.4	13.51	M4.7	. . .	117	. . .
RXJ1147.7-7842	Cha-23	11:47:48.1	-78:41:52.0	10.92	M3.5	. . .	106	. . .
RXJ1149.8-7850	Cha-18; DZ Cha	11:49:31.8	-78:51:01.1	11.01	M0	. . .	110	. . .
RXJ1150.4-7704	Cha19,rej	11:50:28.3	-77:04:38.0	10.54	K4	. . .	. . .	. . .
RXJ1150.9-7411	Cha-24; BRR 15	11:50:45.2	-74:11:13.0	12.06	M3.7	. . .	108	0.91
2MJ11550485-7919108	Cha-25	11:55:04.9	-79:19:10.9	13.26	M3	. . .	115	. . .
T Cha	Cha-26; HIP 58285	11:57:13.5	-79:21:31.5	10.28	K0	107 ± 7	108	. . .
RXJ1158.5-7754B	Cha-20;	11:58:26.8	-77:54:45.0	11.81	M3	. . .	119	. . .
RXJ1158.5-7754A	Cha-21; HIP 58400	11:58:28.2	-77:54:29.6	9.76	K4	90 ± 5	104	0.03
HD 104036	Cha-27; EE Cha	11:58:35.2	-77:49:32.0	6.49	A7	108 ± 8	108H	0.63*
CXOUJ115908.2-781232	Cha-1,cand	11:59:08.0	-78:12:32.2	13.83	M4.75	. . .	165	. . .
ϵ Cha	Cha-2; HJ 4486	11:59:37.5	-78:13:18.9	5.39	B9	. . .	111H	Triple
RXJ1159.7-7601	Cha-28; HIP 58490	11:59:42.3	-76:01:26.2	10.18	K4	101 ± 5	107	. . .
HD 104237A	Cha-5; GRY 1	12:00:05.1	-78:11:34.6	6.31	A7.75	104 ± 6	114H	1.39

Table 1 continued

Table 1 (continued)

NAME	Membership	RA(J2000)	DEC(J2000)	I_c	SpT	Distance[a]	Distance[b]	Sep.
	Other ID	(h : m : s)	(° : ′ : ″)	(mag)		(pc)	(pc)	(″)
(1)	(2)	(3)	(4)	(5)	(6)	(7)	(8)	(9)
HD 104237D	Cha-6; FGL 2	12:00:08.3	-78:11:39.6	11.62	M3.5	. . .	114H	4.2
HD 104237E	Cha-7; FGL 2	12:00:09.3	-78:11:42.5	10.28	K5.5	. . .	114H	. . .
2MJ12005517-7820296	Cha-10	12:00:55.2	-78:20:29.7	14.0	M5.75	. . .	126	. . .
HD 104467	Cha-29	12:01:39.1	-78:59:16.9	7.81	G3	95 ± 6	102	. . .
USNOB 120144.7-781926	Cha-8	12:01:44.4	-78:19:26.8	13.72	M5	. . .	100	. . .
CXOUJ120152.8-781840	Cha-9	12:01:52.5	-78:18:41.4	13.52	M4.75	. . .	121	. . .
RXJ1202.1-7853	Cha-30	12:02:03.8	-78:53:01.0	10.49	M0	. . .	110	0.05*
RXJ1202.8-7718	Cha-cand	12:02:54.6	-77:18:38.2	11.9	M3.5	. . .	128	. . .
RXJ1204.6-7731	Cha-31	12:04:36.1	-77:31:34.6	11.25	M3	. . .	112	. . .
TYC 9420-676-1	Cha-rej	12:04:57.4	-79:32:04.7	9.73	F0	248 ± 47	. . .	0.65*
HD 105234	Cha-cand	12:07:05.5	-78:44:28.1	7.17	A9	101 ± 5	103H	1.44*
2MJ12074597-7816064	Cha-12,rej	12:07:46.0	-78:16:06.5	13.11	M3.75	. . .	. . .	. . .
RXJ1207.7-7953	Cha-32	12:07:48.3	-79:52:42.0	12.06	M3.5	. . .	111	. . .
HIP 59243	Cha-cand	12:09:07.8	-78:46:53.0	6.56	A6	96 ± 6	94H	1.57*
HD 105923	Cha-33	12:11:38.1	-71:10:36.0	8.31	G8	. . .	112	1.99*
RXJ1216.8-7753	Cha-34	12:16:45.9	-77:53:33.0	11.65	M4	. . .	118	. . .
RXJ1219.7-7403	Cha-35	12:19:43.7	-74:03:57.3	10.95	M0	. . .	112	. . .
RXJ1220.4-7407	Cha-36; KOH 93	12:20:21.8	-74:07:39.4	10.8	M0	. . .	110	0.24
2MJ12210499-7116493	Cha-37	12:21:04.9	-71:16:49.3	10.21	K7	. . .	110	. . .
RXJ1239.4-7502	Cha-38	12:39:21.3	-75:02:39.2	9.21	K3	103 ± 5	100	. . .
RXJ1243.1-7458	Cha-rej; BRR 6	12:42:53.1	-74:58:49.0	12.72	M3.2	. . .	. . .	Triple
CD-69 1055	Cha-39	12:58:25.6	-70:28:49.0	8.89	K0	93 ± 5	99	. . .
CM Cha	Cha-cand	13:02:13.6	-76:37:58.0	11.8	K7	. . .	133	. . .
MP Mus	Cha-40; MP Mus	13:22:07.6	-69:38:12.0	9.18	K1	99 ± 7	101	. . .

[a] Derived from Gaia DR1 parallaxes, (Gaia Collaboration et al. 2016a,b)

[b] From Murphy et al. (2013). An "H" means the parallax is from Hipparcos. Otherwise parallaxes are kinematic.

2.2. Instrument and Observing Method

The speckle observations reported here were obtained on 2016 January 17. The time was allocated through the NOAO program 2015B-0268, C. Briceño Principal Investigator. The sky was clear, with good seeing and a slow wind.

We used the *High-Resolution Camera* (HRCam) – a fast imager designed to work at the 4.1-m SOAR telescope (Tokovinin & Cantarutti 2008). The camera was mounted on the SOAR Adaptive Optics Module (SAM; Tokovinin et al. 2016a).[1] We used the UV laser to correct for turbulence, in order to achieve a deeper magnitude limit and better resolution; this observing mode

was used earlier for screening *Kepler-2* variable stars for companions (Schmitt et al. 2016). The SAM module corrects for atmospheric dispersion and helps to calibrate the pixel scale and orientation of HRCam (see Tokovinin et al. 2015). We used mostly the *I*-band filter ($\lambda_0 = 788$ nm; FWHM=132 nm). The transmission curves of HRCam filters are given in the instrument manual.[2]

After acquiring each target and centering it in the HRCam field, we closed the laser loop. The overhead associated with using the laser guide star (LGS) was only a few seconds when observing multiple targets in the same area on the sky. Once the LGS is centered for one target, no further adjustments are needed for the fol-

[1] http://www.ctio.noao.edu/soar/content/soar-adaptive-optics-module-sam

[2] http://www.ctio.noao.edu/~atokovin/speckle/index.html

lowing targets. The laser switches on when the telescope is slewed to the target (the software that controls laser propagation within authorized time windows takes care of this). Laser interrupts had only a minor effect because the exposure times were short. The high-order AO loop compensates for telescope aberrations and low-altitude turbulence; it automatically maintains the optimum focus. Residual tip and tilt jitter is compensated in the data processing. If we had used a classical CCD imager, also available with SAM, the observations would have been much less efficient because acquisition of off-axis guide stars would be needed for each field. For example, the binary survey using SAM with a classical CCD could cover only 21 targets in one night (Tokovinin 2014); in contrast, the 47 stars of this program were observed in 3.2 hours.

Without the laser, HRCam reaches a magnitude limit of $I \sim 12$ mag under good seeing. SAM provides an increase of ~ 1 magnitude in depth, allowing us to go down to $I \sim 13$ mag targets (Table 1). We used a detector binning of 2×2 that produces an effective pixel scale of 30.46 mas. For each target, we acquired two cubes of 200^2 binned pixels size, covering the field of $6'' \times 6''$, with 400 frames per cube. The exposure time was from 0.1 to 0.2 s per frame, depending on the target brightness (i.e. 40 to 80 s accumulation time per data cube). Then two more cubes were acquired with half the field and a shorter exposure (typically 0.05 to 0.1 s). These extra narrow-field cubes helped to increase the resolution at the expense of sensitivity. Shorter exposures were used for targets brighter than $I = 12$ mag, which were also recorded without binning. Bright stars did not need the laser correction. Acquisition of two data cubes in each mode helps to confirm new detections and avoids artifacts such as occasional cosmic rays spoiling some frames in one of the two cubes.

During these observations, the seeing in the free atmosphere reported by the site monitor was very good, fluctuating around $0''.3$. The total seeing varied between $0''.5$ and $1''$. The SAM AO system successfully compensated low-altitude turbulence and delivered sharp images. The median Full Width at Half Maximum (FWHM) of the re-centered average images in closed loop is $0''.33$, while some data cubes have FWHM less than $0''.25$ and 80% are better than $0''.4$.

Some newly resolved pairs have been re-observed with HRCam on 2017 May 15, this time without the laser and under mediocre seeing. These confirmation measurements prove that even relatively faint companions at $\sim 1''$ separation are not background stars. Otherwise the relatively large proper motion of 40 mas yr^{-1}, directed to the West, would have changed the relative companion positions by $0''.05$, significantly larger than the errors.

2.3. Data processing

The speckle data processing described in Tokovinin et al. (2010a - TMH10) was adapted to the faint stars (see Schmitt et al. 2016). It is illustrated in Figure 1. As a first step, power spectra are calculated from the data cubes. While processing each frame, the bias and scaled dark signals are subtracted. The auto-correlation functions (ACFs) are computed from the power spectra. They are used to detect companions and to evaluate the detection limits. For each data cube, the speckle pipeline also delivers the average image re-centered using optimized center-of-gravity algorithm, and the shift-and-add (SAA) or "lucky" image re-centered on the brightest pixel in each frame, with weight proportional to the signal in this pixel.

Parameters of binary and triple stars are determined by fitting the power spectrum to its model, which is a product of the binary (or triple) star power spectrum and the reference spectrum. We used as a reference the azimuthally-averaged spectrum of the target itself in the case of binaries wider than $0''.1$. For closer pairs, the "synthetic" reference was used (see TMH10). Some data were processed using other observed objects as a reference. If the reference object is a binary, it is converted into a single star by deconvolution, using the measured binary parameters. Photometry of wide (classically resolved) binaries is corrected for speckle anisoplanatism using the centered images. Inspection of the centered and SAA images helped to confirm some companions seen in the ACF.

The relatively long exposure times used for targets fainter than $I_C = 13$ mag reduced the effective resolution to about $0''.1$, while the diffraction-limited resolution of $0''.04$ was reached for the brighter stars. No appreciable image elongation of instrumental origin was noted in the data. Nevertheless, we always compared with stars observed before or after each target to check for such artifacts. The detector orientation and pixel scale were accurately calibrated on wide binaries with well-modeled linear motions (Tokovinin et al. 2015). The calibration parameters are determined with an accuracy of $0°.1$ and 0.1%, respectively.

The detection limits were estimated from the ACFs by computing the variance in annular zones and assuming that companions brighter than 5σ are detectable (see TMH10). Figure 2 shows the detection limits for faint targets observed in closed loop. They vary substantially, depending on the target brightness and AO compensation quality. The median magnitude difference ΔI
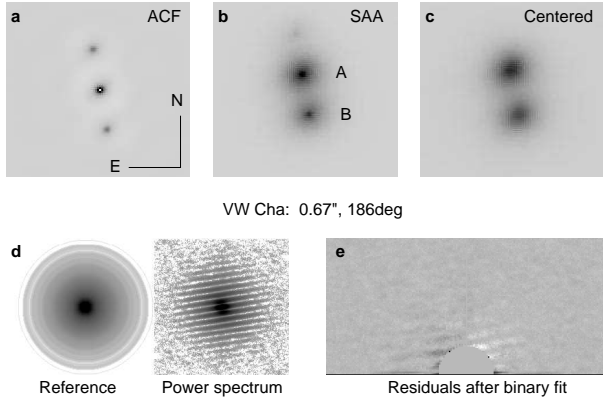
Figure 1. Example of the speckle data processing for the well-resolved binary VW Cha. The rop row shows the central fragments of images, in the negative scale: the ACF (a), the SAA image (b), and the centered image (c). The bottom row shows the data in the Fourier space: the power spectrum and the reference spectrum in the negative logarithmic scale (d) and the residuals after fitting with the binary-star model in the linear scale (e). As the power spectrum is symmetric, only the upper half of the frequency plane is fitted; the low spatial frequencies are masked out.
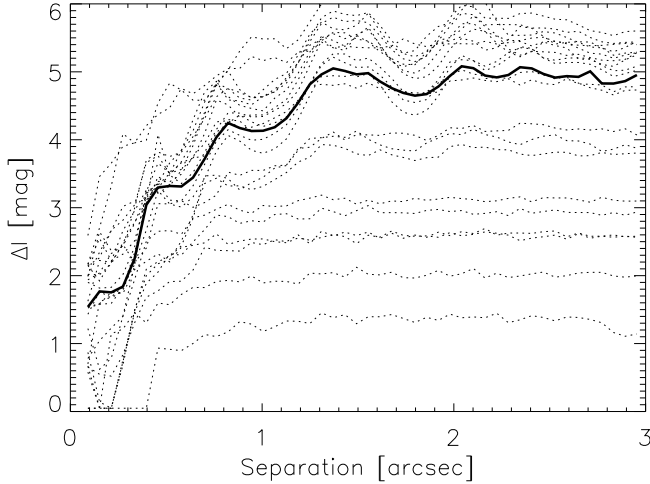
Figure 2. Detection limits for 20 faint unresolved targets recorded with 2×2 binning and 0.1 s exposure time. The thick curve shows the median detection limit while the dotted lines are the individual limits.

at 0″.15 separation is 1.75 mag, while at 1″ separation it reaches 4 mag. Individual ΔI limits at these two characteristic separations are provided in Table 3 for unresolved targets. Linear interpolation between these points can be used to get the detection limits at other separations.

3. RESULTS

Figure 3 shows centered or SAA images of six newly resolved binaries. Another three new close pairs are il-
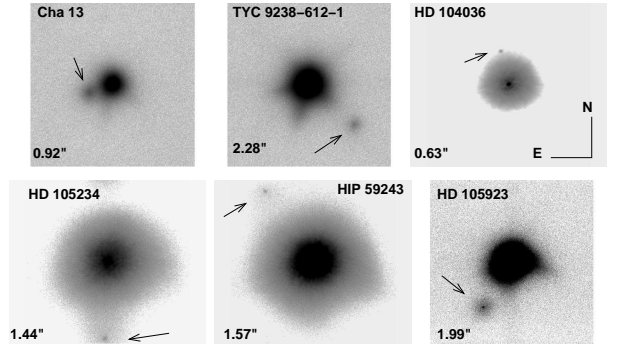
Figure 3. Images of six newly resolved binaries with faint companions displayed on arbitrary negative scale. The separation is indicated in the lower left corner of each image, the companions are marked by arrows. **Cha-13 and TYC 9238-612-1** are average images in closed AO loop, the rest are SAA images with or without AO.
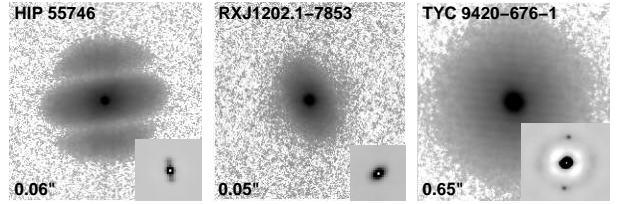

Figure 4. Power spectra of three resolved close binaries displayed on the logarithmic scale. The separation is indicated in the lower left corner; **the inserts in the lower right corners show the central fragments of the ACFs.**

lustrated in Figure 4 by their power spectra showing fringes or elongation.

Table 2 lists 31 measures of 20 binary pairs, including 10 newly resolved ones. The columns of Table 2 contain (1) the WDS-style code based on the J2000 coordinates; (2) the star name, from Table 1 in Murphy et al. (2013), (3) the Besselian epoch of observation, (4) the filter used, (5) the position angle θ in degrees, (6) the separation ρ in arcseconds, (7) the magnitude difference Δm, with an asterisk following if Δm and the true quadrant are determined from the resolved long-exposure image; a colon indicates that the data are noisy and Δm is likely overestimated (see TMH10 for details); the flag 'q' means that the quadrant is determined from the SAA image. In cases of multiple stars, the positions and photometry refer to the pairings between individual stars, not the photocenters of subsystems. The last column (8) gives short notes for some objects.

Table 2. Measurements of resolved multiples in ϵ Cha

WDS	Name	Epoch +2000	Filter	θ (°)	ρ ('')	Δm (mag)	Note
11080−7742	VW Cha; GHE 35 AB	16.0474	I	185.9	0.6670	0.2 *	
11186−7936	Cha 13	16.0475	I	107.8	0.9218	3.2 *	
11253−8457	HIP 55746	16.0475	I	184.9	0.0614	0.6 q	
		16.0475	y	185.2	0.0607	0.9 q	
		16.9595	y	187.1	0.0525	0.3	
		16.9595	I	188.4	0.0489	0.4	
11375−7648	RXJ1137.4-7648	16.0475	I	5.5	2.8952	1.8	
11415−7347	TYC 9238-612-1	16.0475	I	226.1	2.2767	5.7 *	
		17.3719	I	226.3	2.2620	5.3 :	
11509−7411	RXJ11509-7411; BRR 15	16.0475	I	105.3	0.9143	1.7 *	
11585−7749	HD 104036; Cha 27	16.0475	I	10.9	0.6304	3.6 *	
		16.0475	y	10.9	0.6295	4.9 q	
		17.3718	I	10.8	0.6383	3.7 q	
11585−7754	RXJ115805-7754A; KOH 91	16.0475	I	147.7	0.0306	1.0 :	Marginal
11596−7813	ϵ Cha; HJ 4486 Aa,Ab	16.0475	y	47.6	0.0592	0.2	Triple
		17.3717	y	28.8	0.0612	0.2	
11596−7813	ϵ Cha; HJ 4486 Aa,B	16.0475	y	239.0	0.1779	0.1	Triple
		17.3717	y	247.0	0.1731	0.0	
12001−7812	HD 104237A; GRY 1 AF	16.0475	I	254.8	1.3904	5.5 *	
12001−7811	HD 104237D; FGL 2 ED	16.0477	I	311.3	4.2409	1.9	
12021−7853	RX J1202.1-7853; Cha 30	16.0475	I	111.9	0.0521	1.2	Tentative
12049−7932	TYC 9420-676-1	16.0476	I	172.3	0.6565	3.4 *	
		17.3718	I	172.3	0.6605	3.7	
12070−7844	HD 105234	16.0476	I	175.0	1.4408	4.4 *	
		17.3718	I	174.7	1.4303	5.6 *	
12091−7846	HIP 59243	16.0476	I	31.7	1.5676	5.6 *	
12116−7110	HD 105923	16.0476	I	145.5	1.9893	4.7 *	
12204−7407	RXJ1220.4-7407; KOH 93	16.0476	I	9.4	0.2446	1.8 q	
		17.3719	I	12.1	0.2448	1.2 :	
12431−7458	RXJ1243.1-7458; BRR 6 Aa,B	16.0477	I	258.1	2.5246	2.5	Triple
12431−7458	RXJ1243.1-7458; KOH 94 Aa,Ab	16.0477	I	79.8	0.2379	1.3 q	Triple

Table 3 lists the detection limits for unresolved targets. The minimum separation $\rho_{\min}$ in column 2 equals the diffraction limits of 40 mas for all targets except the faintest ones, where it is 0.''1. The following columns give the maximum detectable magnitude difference in the I band at separations of 0.''15 and 1'', estimated from the ACF. Note that the detection limits in Figure 2 refer only to the large binned data cubes, whereas those in Table 3 are the deepest limits for each target in all observing modes.

Overall, we measured eight known systems (including three triples, of which we confirmed two) and added ten new binary pairs resolved here for the first time. The following Subsection 3.1 gives comments on individual binaries, the Subsection 3.2 is devoted to the multiple system ϵ Cha itself.

3.1. *Comments on resolved systems in ϵ Cha*

11080-7742. VW Cha (GHE 35 AB) is a K7-M0 accreting Classical T Tauri star, classified as a Class II object based on its Spectral Energy Distribution (SED;

Table 3. Detection limits for unresolved targets

Name	ρ_{min}	$\Delta m(0''15)$	$\Delta m(1'')$
	('')	(mag)	(mag)
HD 82879	0.04	1.6	5.1
CP-68 1388	0.04	2.2	4.8
TYC 9414-191-1	0.04	1.6	4.3
RXJ1123.2-7924	0.04	1.9	3.4
2MJ11432669-78...	0.10	0.9	2.2
RXJ1147.7-7842	0.04	1.7	4.0
RXJ1149.8-7850	0.04	2.1	4.3
RXJ1150.4-7704	0.04	1.8	4.6
2MJ11550485-79...	0.10	1.7	3.3
T Cha	0.04	2.4	5.1
RXJ1158.5-7754B	0.04	2.0	4.2
CXOUJ115908	0.10	2.2	2.3
HD 104237E	0.04	1.6	4.6
2MJ12005517-78...	0.04	1.4	2.6
HD 104467	0.04	0.7	6.1
USNOB-120144-78...	0.10	2.0	2.9
CXOUJ120152-78...	0.10	2.0	3.2
RXJ1202.8-7718	0.04	2.5	4.5
RXJ1204.6-7731	0.04	2.3	4.5
2MJ12074597	0.10	2.5	3.6
RXJ1207.7-7953	0.04	2.6	3.9
RXJ1216.8-7753	0.04	2.4	4.6
RXJ1219.7-7403	0.04	1.8	4.2
2MJ12210499-71..	0.04	1.7	5.1
RXJ1239.4-7502	0.04	1.9	5.3
CD-69 1055	0.04	0.7	5.2
CM Cha	0.04	2.2	4.4
MP Mus	0.04	2.1	4.9

Manoj et al. 2011). This system is resolved at 0''66, without any trace of the 0''1 subsystem BNK 1 Ba,Bb discovered by Brandeker et al. (2001) in 2000. The subsystem Ba,Bb was also unresolved at SOAR in 2014 and 2015, although at $\Delta J = 0.3$ mag it should be easily detectable. It is possible that the pair Ba,Bb became closer (its estimated period is ∼70 yr). The pair AB moved very little since its discovery in 1994; its estimated period is ∼400 yr. Not a member of the association, but definitely a young object; Murphy et al. (2013) attribute it to the Cha I group. It is not featured in the *Gaia* DR1 so its true membership is still difficult to ascertain.

11186-7936. 2MASS J11183572-7935548 (Cha 13, $I =$ 12.22 mag, M4.5) is a new 0''92 binary. Murphy et al. (2013) suspected RV variability, which might mean that it is triple, because the new wide pair has a period of ∼2 kyr. In their Spitzer study of Chamaeleon, Manoj et al. (2011) classify this star as a Weak-lined T Tauri star based on the modest Hα emission equivalent width of 11Å reported in literature low resolution spectra. However, the Spectral Energy Distribution (SED) clearly shows this is not a disk-less star, quite the contrary. Though it has a stellar-like SED out to ∼ 3 μm, it exhibits significant excess emission at longer wavelengths, with a strong 10 μm silicate emission feature, indicative of a small amount of optically thin dust in an otherwise cleared gap; thus, they classify it as a candidate Transitional Disk (TD). Murphy et al. (2013) also find that Hα is variable in Cha-13, though the line profile itself is not very wide, with a 10% width of ∼ 170 km s^{-1}, consistent with a low accretion rate of ∼ 10^{-11}M$_\odot$ yr^{-1}. These characteristics closely resemble those of other TDs, like CVSO-224 in Orion (Espaillat et al. 2008). In addition to Hα, Murphy et al. (2013) find a number of other emission lines in their spectra of Cha-13, like He I, [NII]λ6548/6583, [SII]λ6716/6731, among others, leading them to suggest the gap may have been cleared by jet/outflow activity. Our discovery of a companion at ∼ 90 AU raises the alternative interpretation that the TD status is related to the binary nature of the system. At separations of ≲ 200 AU a companion can truncate the outer disk, while at separations of ≲ few tens of AU the disk could be truncated from the inside (Manoj et al. 2011). Indeed, studying Chamaeleon I Daemgen et al. (2016) find that there is a statistically significant difference in the accretor fraction between single and binary systems; in particular, binary systems with separations ≲ 100 AU show a low ∼ 6% incidence of accretion activity. More specifically, a recent study of 24 TDs shows that close to 38% can be explained by tidal interactions between a close binary companion and its disk, while the rest is likely the result of processes like disk photoevaporation, grain growth or planet-disk interactions (Ruíz-Rodríguez et al. 2016). Does the weak accretion activity and excess infrared emission in Cha-13 originate in one or two circumprimary disks, or maybe in a circumbinary disk? Has the gap in this TD system been carved out by the binary companion? These are open questions for this very interesting system that clearly deserves further detailed studies.

11253-8457. HIP 55746 is revealed as a tight 60-mas binary with an estimated period of ∼10 yr. This close pair was suspected from the astrometric acceleration detected by *Hipparcos* (Frankowski et al. 2007). The pair

was resolved again at SOAR in 2016.96 and closed down to about 30 mas in 2017.34 (the elongated power spectrum was not fitted, no measurement). There is another companion at 3″.54 (RST 2752), so the system is triple. The wide physical companion, last seen in 1996 at (208°, 3″.5), is outside the field of view, hence it is not detected here.

11375-7648. RX J1137.4-7648 ($I = 12.2$ mag, M2), not a member of ε Cha, has a wide 2″.9 companion that just fits in the 6″ field. Its image is partially truncated, so the ΔI is over-estimated by some unknown amount. Although Murphy et al. (2013) call it "equal-brightness visual binary", and it is evident as a visual pair in Digitized Sky Survey (DSS) and 2 Micron All-Sky Survey (2MASS) images, this pair is not featured neither in the literature nor in the WDS.

11415-7347. TYC 9238-612-1 ($I = 9.98$ mag, G5) has a faint companion at 2″.28. It is barely detectable at the same position in 2017.37.

11509-7411. RX J1150.9-7411 is a previously known binary BRR 15, resolved here at 0″.91. It has not moved appreciably since its discovery in 1994. Köhler (2001) found it at 0″.875 and 106°.0.

11585-7749. HD 104036 ($I = 6.49$ mag, A7) has a new faint companion at 0″.63. The pair is found at the same position in 2017.37, confirming that the companion is physical. The new companion is too distant for explaining the RV variability suspected by Murphy et al. (2013).

11585−7754. The close binary KOH 91 (Cha-21) is marginally resolved at 30 mas. Although the resolution is tentative, this is the only confirmation of the original discovery made by Köhler at separation 0″.073 and magnitude difference $\Delta K = 0.75$ mag. The system is triple considering the faint companion RXJ1158.5-7754B at 16″.6 distance. The estimated period of AB is 30 kyr.

12001-7811. HD 104237 ($I = 6.31$), an accreting Herbig Ae spectroscopic binary with a circumbinary disk, is surrounded by several faint stars, forming a kind of mini-cluster (Grady et al. 2004). We resolved the closest 1″.4 pair AF[3] and measured the 4″.24 pair ED owing to its favorable orientation along the diagonal of the detector. HD 104237 is located at 135″ from the ε Cha and

is listed in the WDS as its companion C, although the orbital period of such a wide pair AB,C would be on the order of 0.5 Myr. The 19-day inner spectroscopic binary resolved interferometrically by Garcia et al. (2013) has a semimajor axis of 2 mas, well below the SOAR resolution limit. Not surprisingly, our observations do not reveal any additional close companions to HD 104237 itself and to two of its satellites because these objects are already well studied.

12021−7853. RX J1202.1-7853 ($I = 10.5$ mag, M0) has an elongated power spectrum corresponding to a 50-mas binary (Figure 4). The resolution is tentative, but likely real by comparison with other targets that do not show similar elongation. This star was observed by Köhler (2001) but not resolved, being below the diffraction limit of 0″.13. The RV variability found by Murphy et al. (2013) could be caused by the new close companion.

12049−7932. TYC 9420-676-1 ($I = 9.7$ mag, F0) has a new companion at 0″.65, confirmed as physical by its repeated measurement in 2017.37. According to Murphy et al. (2013) it does not belong to the association.

12070−7844. HD 105234 ($I = 7.2$ mag, A9) has a new 1″.44 companion, confirmed as physical in 2017.37.

12091-7846. HIP 59243 ($I = 6.56$ mag, A6) is resolved at 1″.57. The binary is very likely physical, but there is no second measure to confirm this.

12116−7110. HD 105923 ($J = 8.3$ mag, G0) has a faint companion at 1″.99. Elliott et al. (2015) also detected this binary in 2006 at 1″.96 and 145°.1. The companion is thus physical.

12204-7407. RX J1220.4-7407 ($I = 10.80$ mag, M0) is a known binary KOH 93. It was discovered in 1996 at (348°.4, 0″.296) by Köhler (2001). It is found here at (9°.3, 0″.24). The estimated period is ∼140 yr; the observed direct motion (21° in 30 yr) matches this crude estimate. According to Murphy et al. (2013), the star RX J1219.77403 at a projected separation of 0.14 pc could be bound to this binary, thus making it triple system.

12431-7459. RX J1243.1-7458 ($I = 12.72$ mag, M3.2), not a member of ε Cha, is resolved as a triple system consisting of the close 0″.23 pair and a fainter companion at 2″.5. This triple is already known, designated in the WDS as KOH 94 Aa,Ab and BRR 6 AB. The inner subsystem was discovered in 1996 at (85°, 0″.3) (Köhler 2001) and not measured since. It is found at (78°.3, 0″.23). The orbital motion is slow. Murphy et al. (2013) note a possible spectroscopic companion, which, if true, would make this a quadruple system. They assign this system to the more distant Cha II cloud population.

---

[3] **The WDS component F corresponds to the "star 2" in Grady et al. (2004) and is sometimes called "B", causing confusion with the 4″.1 pair FGL 2AB listed in the WDS, which is erroneous and unphysical. Based on the images presented by Grady et al. (2004) and Feigelson et al. (2003), the close AF pair is the same as the AB pair described by Feigelson et al. (2003), and there is no 4.1″ A-? pair among the known components. The WDS AB pair appears to be a historical artefact.**

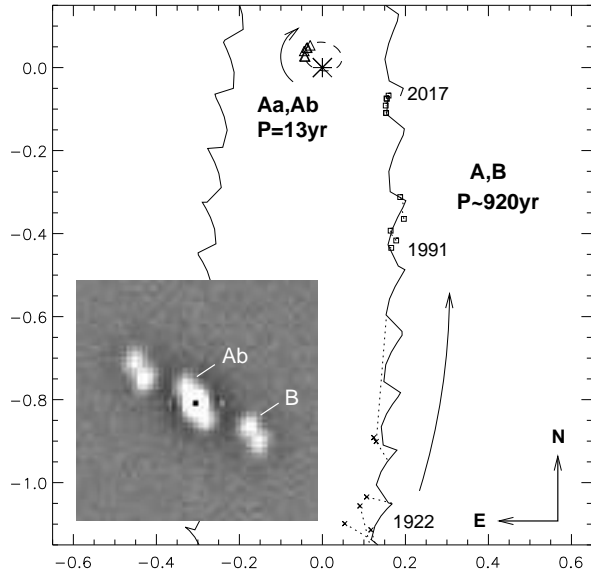## 3.2. The triple system ε Cha

Figure 5. Tentative orbits of the triple system ε Cha with axis scale in arcseconds. Only a fragment of the outer orbit is plotted; its wavy trajectory reflects the wobble caused by the inner subsystem. **Crosses and squares connected to the orbit by dotted lines denote the measurements of the outer pair, with some dates indicated (the first measurement made in 1835 is outside the plot). Triangles mark the measurements of the inner pair.** The insert shows the ACF recorded at SOAR on 2017 May 15 **where Ab and B mark the peaks corresponding to the two companions.**

The central star of the association, ε Cha (HIP 58474, HD 104174, B9V), is a known binary, HJ 4486, discovered in 1835 by Hershel (1847) at a separation of 1″6 and position angle 179°. Since the discovery, the separation of the bright companion B has steadily decreased to the present 0″17, with a slow increase of the position angle to 240°. In 2015, the system was observed at SOAR and unexpectedly resolved into a tight triple with nearly equal components (Tokovinin et al. 2016b).

The inner 50-mas pair has turned by 29° in two years since its discovery, in agreement with its estimated short period. Figure 5 shows the tentative orbits of the outer and inner pairs computed from the available data. These orbits, still quite uncertain, are given here only as an illustration; they are not yet ready for publication. The provisional orbits match the expected masses of these stars, about 2.5 M⊙ each. The short inner period means that the inner orbit will be constrained in a few more years, while the millennium-long outer orbit will remain uncertain for the lack of coverage. Accurate speckle measurements at SOAR begin to show the "wobble" in

the relative position of Aa and B caused by the subsystem. The amplitude of the wobble is about half of the inner semimajor axis because the components Aa and Ab have comparable masses. Future monitoring of this interesting triple system will allow accurate measurements of the masses of these young B9V stars and will provide a valuable anchor point for stellar evolutionary models.

Interestingly, the inner and outer pairs in ε Cha rotate in opposite directions. The provisional orbits are almost orthogonal, while the inner orbit has a large eccentricity of ∼0.8. This triple system may be undergoing Lidov-Kozai cycles that might lead to the formation of a close inner binary (see the review by Naoz 2016).

4. DISCUSSION: THE MULTIPLICITY FRACTION

The multiplicity strongly depends on the mass (Duchêne & Kraus 2013). To be meaningful, the observationally determined multiplicity fraction must refer to the well-defined range of primary masses, separations (or periods), and mass ratios. However, masses and mass ratios are notoriously difficult to estimate for PMS stars. As the small sample size does not allow accurate multiplicity measurement in ε Cha, crude qualitative estimates of the multiplicity fraction given below seem to be appropriate. Owing to the limited observational material, we prefer not to speculate about the multiplicity statistics in ε Cha or compare with other young groups.

We select from Table 1 thirty members and candidate members of ε Cha with spectral types of G0 or later ($I > 8$ mag) for comparison with the field dwarfs. There are 6 binaries in the projected separation range from 4 to 300 AU (1.9 dex). All those companions are physical. This leads to a raw multiplicity fraction of 0.10±0.04 per decade of separation. As we have not sampled the full range of mass ratios owing to the separation-dependent detection limit, the actual multiplicity fraction is higher, but this correction depends on the mass ratio distribution and is highly uncertain. Within errors, the multiplicity of low-mass stars in ε Cha appears to be comparable to the multiplicity fraction of solar-type dwarfs in this separation range, about 0.15 per decade (Duchêne & Kraus 2013).

We have not detected any companions to the four targets fainter than $I = 13$ mag. However, the detection limits for faint stars are not very deep, while the number of those low-mass members is too small to make any conclusions regarding multiplicity dependence on mass. The faintest resolved association member, Cha-13, has $I = 12.2$ mag and spectral type M4.5.
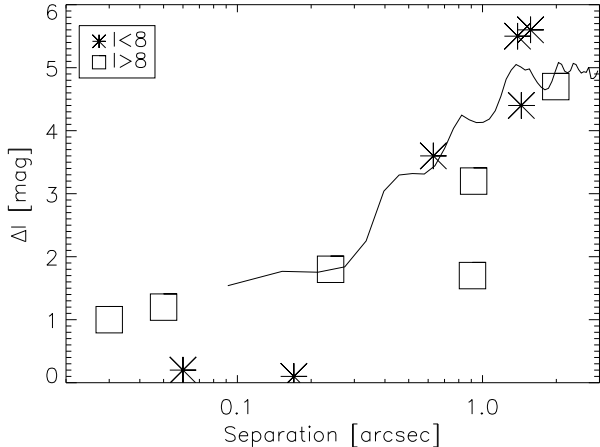
Figure 6. Binary companions to the members of ε Cha association: magnitude difference vs. separation. Squares denote stars of moderate mass fainter than $I = 8$ mag, asterisks stand for five more massive and brighter members of the association. The median detection limit for faint targets is plotted in full line.

Among the five massive association members with spectral types A and B ($I < 8$ mag), we find a total of 6 companions in the the surveyed separation range (4 to 300 AU), leading to the multiplicity fraction of 1.2 (0.6 per decade of separation). Four of those massive stars (HD 104036, HD 104237, HD 105234, and HIP 59243) have low-mass companions at separations larger than 60 AU. Only ε Cha itself stands out, being composed of three nearly equal B9V stars.

Figure 6 plots separations of the binary association members on the logarithmic scale and compares them to the median detection limit from Figure 2. Several faint companions with separations of the order of $1''$ are close to the limit and would have been missed if they were much closer. Interestingly, in Figure 3 of Köhler (2001) there are also several binaries with separations between $0\rlap{.}''3$ and $6''$ and faint companions (flux ratios less than 0.3 in the K band), as well as a distinct group of binaries with smaller separations and roughly equal components. There may be a similar pattern in Figure 6, where all close binaries have small ΔI. It would be interesting

to probe the presence or absence of close and low-mass companions with a high-contrast AO, as our detection limits at small separations are not deep enough.

We can't help noting that our relatively small sample contains five young triple systems (not all of them are association members).

In summary, our work contributes new observational material on the binary statistics in young associations and clusters. The ε Cha association appears to be different in this respect from the neighboring η Cha cluster, where Becker et al. (2013) noted the lack of low-mass stars (a top-heavy IMF) as well as the absence of binaries with separations above 20 AU.

Facility: SOAR.

REFERENCES

Becker, C., Moraux, E., Duchêne, G. et al. 2013, A&A, 552, 46

Brandeker, A., Liseau, R., Artymowicz, P., & Jayawardhana, R. 2001, ApJ, 561, L199

Correia, S., Zinnecker, H., Ratzka, Th., & Sterzik, M. F. 2006, A&A, 459, 909

Daemgen, S., Elliot Meyer, R., Jayawardhana, R., & Petr-Gotzens, M. G. 2016, A&A, 586, A12

Duchêne, G. & Kraus, A. 2013, ARA&A, 51, 269

Elliott, P., Huelamo, N., Bouy, H. et al. 2015, A&A, 580, 88

Espaillat, C., Muzerolle, J., Hernández, J., et al. 2008, ApJL, 689, L145

Feigelson, E. D., Lawson, W. A., & Garmire, G. P. 2003, ApJ, 599, 1207

Frankowski, A., Jancart, S., Jorissen, A. 2007, A&A, 464, 377

Frink, S., Roeser, S., Alcala, J. M. et al. 1998, A&A, 338, 442

Gaia Collaboration, Brown, A. G. A., Vallenari, A., et al. 2016a, A&A, 595, A2

Gaia Collaboration, Prusti, T., de Bruijne, J. H. J., et al. 2016b, A&A, 595, A1

Garcia, P. J. V., Benisty, M., Dougados, C. et al. 2013, MNRAS, 430, 1839

Grady, C. A., Woodgate, B., Torres, C. A. O. et al. 2004, ApJ, 608, 809

Herschel, J. F. W. 1847, Cape Results, London

King R. R., Parker, R. J., Patience, J, & Goodwin, S. P. 2012, MNRAS, 421, 2025

Köhler, R. 2001, AJ, 122, 3325

Köhler, R., Petr-Gotzens, M. G., McCaughrean, M. J. et al. 2006, A&A, 458, 461

Kroupa, P. 1995, MNRAS, 277, 1491

Kroupa, P. et al. 1999, New Astron., 4, 495

Kroupa, P. and Petr-Gotzens, M. 2011, å, 529, 92

Lindegren, L., Lammers, U., Bastian, U. et al. 2016, A&A, 595, 4

Mamajek, E. E., Lawson, W. A., & Feigelson, E. D. 1999, Bulletin of the American Astronomical Society, 31, 53.11

Mamajek, E. E., Lawson, W. A., & Feigelson, E. D. 2000, ApJ, 544, 356

Manoj, P., Kim, K. H., Furlan, E., McClure, M. K., Luhman, K. L., Watson, Dan M., Espaillat, C., Calvet, N., Najita, J. R., D'Alessio, P., Adame, L., Sargent, B. A., Forrest, W. J., Bohac, C., Green, J. D., Arnold, L. A. 2011, ApJS, 193, 11

Marks, M., Leigh, N., Giersz, M., Pfalzner, S., Pflamm-Altenburg, J., & Oh, S. 2014, MNRAS, 441, 3503

Mason, B. D., Wycoff, G. L., Hartkopf, W. I. et al. 2001, AJ, 122, 3466 (WDS)

Murphy, S. J., Lawson, W. A., & Bessell, M. S. 2013, MNRAS, 435, 1325

Naoz, S. 2016, ARAA, 54, 441

Parker, R. J. & Meyer, M. 2014, MNRAS, 442, 3722

Petr, M., Coudé du Foresto, V., Beckwith, S. V. W. et al. 1998, ApJ, 500, 825

Reipurth, B., Clarke, C. J., Boss, A. P. et al. 2014, in Protostars and Planets VI, Henrik Beuther, Ralf S. Klessen, Cornelis P. Dullemond, and Thomas Henning (eds.), University of Arizona Press, Tucson, p.267-290

Ruíz-Rodríguez, D., Ireland, M., Cieza, L., & Kraus, A. 2016, MNRAS, 463, 3829

Schmitt, J. R., Tokovinin, A., Wang, Ji, et al. 2016, AJ, 151, 159

Tokovinin, A. & Cantarutti, R. 2008, PASP, 120, 170

Tokovinin, A., Mason, B. D., & Hartkopf, W. I. 2010, AJ, 139, 743 (TMH10)

Tokovinin, A. 2014, AJ, 148, 72

Tokovinin, A., Mason, B. D., & Hartkopf, W. I. et al. 2015, AJ, 150, 50

Tokovinin, A., Cantarutti, R., Tighe, R. et al. 2016a, PASP, 128, 125003

Tokovinin, A., Mason, B. D., & Hartkopf, W. I. et al. 2016b, AJ, 151, 153

Tokovinin, A. 2016, AJ, 152, 138

Torres, C. A. O., Quast, G. R., Melo, C. H. F., & Sterzik, M. F. 2008, in Handbook of Star Forming Regions, Volume II: The Southern Sky ASP Monograph Publications, Vol. 5. Edited by Bo Reipurth, p.757

Zuckerman, B., & Song, I. 2004, ARA&A, 42, 685